RESEARCH PAPER

Aptamer-based electrochemical biosensing strategy toward human non-small cell lung cancer using polyacrylonitrile/polypyrrole nanofibers

Ezgi Kivrak[1,4] · Atike Ince-Yardimci[2] · Recep Ilhan[3] · Petek Ballar Kirmizibayrak[3] · Selahattin Yilmaz[2] · Pinar Kara[1]

Abstract

In the present study, a sensitive electrochemical aptamer-based biosensing strategy for human non-small cell lung cancer (NSCLC) detection was proposed using nanofiber-modified disposable pencil graphite electrodes (PGEs). The composite nanofiber was comprised of polyacrylonitrile (PAN) and polypyrrole (PPy) polymers, and fabrication of the nanofibers was accomplished using electrospinning process onto PGEs. Development of the nanofibers was confirmed using scanning electron microscopy (SEM). The high-affinity 5′-aminohexyl-linked aptamer was immobilized onto a PAN/PPy composite nanofiber-modified sensor surface via covalent bonding strategy. After incubation with NSCLC living cells (A549 cell line) at 37.5 °C, the recognition between aptamer and target cells was monitored by electrochemical impedance spectroscopy (EIS). The selectivity of the aptasensor was evaluated using nonspecific human cervical cancer cells (HeLa) and a nonspecific aptamer sequence. The proposed electrochemical aptasensor showed high sensitivity toward A549 cells with a detection limit of 1.2×10^3 cells/mL. The results indicate that our label-free electrochemical aptasensor has great potential in the design of aptasensors for the diagnostics of other types of cancer cells with broad detection capability in clinical analysis.

Keywords Aptasensor · Early cancer diagnosis · Non-small cell lung cancer · Electrochemical impedance spectrometry · Nanofibers

Introduction

Cancer is still the major cause of death worldwide, along with cardiovascular diseases [1]. A recent World Health Organization (WHO) report on cancer shows that there were 9.6 million cancer-related deaths in 2018, and 1.76 million of the deaths were caused by lung cancer [2].

Lung cancer is divided into two main histological subtypes, small cell lung carcinoma (SCLC) and non-small cell lung carcinoma (NSCLC), accounting for 15% and 85% of all lung cancer types, respectively [3]. Screening, early-stage detection and proper treatment of metastases are very crucial in terms of reducing the cancer burden [4].

Several screening methods have commonly been used, including computed tomography (CT), magnetic resonance imaging (MRI), positron emission tomography (PET) and chest radiograph (CRG), but these techniques lack sensitivity for the detection of cancer cells at premalignant stages [5, 6]. Thus, new methodologies are needed for early-stage diagnosis of cancer.

There has been growing research interest in the development of rapid, reliable and ultrasensitive cancer detection methods for clinical analysis. Among the available techniques, aptamer-based biosensing methods have shown great promise due to their high sensitivity and selectivity for the target biomolecules.

✉ Pinar Kara
pinar.kara@ege.edu.tr

1 Faculty of Pharmacy, Department of Analytical Chemistry, Ege University, 35100 Izmir, Bornova, Turkey

2 Izmir Institute of Technology, Department of Chemical Engineering, 35430 Urla, İzmir, Turkey

3 Faculty of Pharmacy, Department of Biochemistry, Ege University, 35100 Izmir, Bornova, Turkey

4 Graduate School of Natural and Applied Sciences, Department of Biomedical Technologies, Ege University, 35100 Izmir, Bornova, Turkey

Aptamers, namely chemical antibodies, are artificial single-stranded DNA (ssDNA) and RNA nucleic acids that were discovered and characterized almost 30 years ago. Aptamers have been used in many fields due to their high affinity and specificity toward target molecules by folding into tertiary structures [7–9]. Although aptamers are functionally similar to antibodies, they have some significant advantages over them, such as an in vitro selection process known as SELEX (Systematic Evolution of Ligands by Exponential Enrichment), short production time and cost-effectiveness, less variability between batches, reversibility after thermal denaturation, low immunogenicity, small size [10] and a broad range of potential targets, from proteins [11, 12] and toxins [13, 14] to whole cells [15–17]. In addition, aptamers have been used in clinical diagnostics along with biomarker discovery, controlled drug release and targeted therapy [18].

Aptamer-based biosensors, or "aptasensors," are a promising diagnostic tool for clinical analysis using aptamers as biorecognition elements in biosensors [19, 20]. Electrochemical biosensors are based on electrochemical strategies that provide high sensitivity, inherent miniaturization, rapid diagnosis, simple instrumentation and low cost [21–23]. Electrochemical impedance spectroscopy (EIS) is an important and facile analytical tool used in the characterization of physicochemical processes in different stages of electrode modification. The impedance of an electrochemical system is evaluated by applying a small-amplitude AC sinusoidal wave potential as a function of frequency and detecting the change in one impedance element such as resistance or capacitance [24]. In the field of biosensors, EIS is an effective tool for the characterization of surface modifications such as immobilization of biomolecules on electrode surfaces and monitoring their interactions with their target molecules [25]. Moreover, the integration of novel nanomaterials into aptasensors has led to new and improved applications for diagnostic tools. Carbon nanofibers (CNFs) are an attractive material in the area of electrochemical biosensors due to their high surface area, tunable electromechanical properties and high conductivity, and thus rapid electron transfer [26, 27].

Herein, the label-free electrochemical detection of human non-small cell lung cancer (A549 cells), which is one of the most common and fatal types of cancer, was accomplished using a specific aptamer sequence. The 5′-aminohexyl-linked DNA aptamer toward the A549 cell line was selected based on the literature, and was evolved using the cell-based SELEX approach [28]. Polyacrylonitrile (PAN) and polypyrrole (PPy) polymers were used to construct nanofibers on disposable pencil graphite electrodes (PGEs). The nanofiber-modified PGE (NFPGE) was partially hydrolyzed with a NaOH aqueous solution to convert the nitrile groups of the nanofiber into carboxyl groups. The aptamer sequence was immobilized onto the functionalized NFPGE (f-NFPGE) surface covalently via carbodiimide chemistry. Human cervical cancer cells (HeLa) were used as negative control. The binding of cancer cells onto aptamer-modified electrode surfaces at 37.5 °C was monitored by electrochemical impedance spectroscopy (EIS) transduction of the charge transfer resistance (R_{ct}) in the presence of 5 mM $[Fe(CN)_6]^{3-/4-}$. Electrode characteristics were evaluated using scanning electron microscopy (SEM).

Materials and methods

Chemicals and reagents

N-hydroxysuccinimide (NHS), 1-ethyl-3-(3-dimethylaminopropyl) carbodiimide hydrochloride (EDC), polyacrylonitrile (PAN), polypyrrole 5 wt% dispersion in H_2O (PPy), N,N-dimethylformamide (DMF) and diethanolamine (DEA) were purchased from Sigma-Aldrich (Germany).

The A549 cell specific aptamer sequence was synthesized by Ella Biotech, Germany. The sequence of the oligonucleotide was as follows:

5′-NH$_2$-(CH$_2$)$_6$-GGT TGC ATG CCG TGG GGA GGG GGG TGG GTT TTA TAG CGT ACT CAG-3′.

To assess selectivity, a nonspecific aptamer sequence was used, and the sequence of the oligonucleotide was given as:

5′-NH$_2$-(CH$_2$)$_6$-GAT CGG GTG TGG GTG GCG TAA AGG GAG CAT CGG ACA-3′.

All stock solutions of the aptamers (1000 μg/mL) and buffers were prepared with ultrapure water (18 MΩ, Millipore), and the aptamers were divided into aliquots to be kept frozen at −20 °C. Individual dilutions of the aptamer solutions were prepared in 0.50 M acetate buffer solution (ABS) containing 0.50 M acetic acid and 20 mM NaCl pH = 4.8).

All cell lines were diluted to desired concentrations with 0.05 M phosphate-buffered saline (PBS) solution containing 500 mM NaCl (pH = 7.4).

Apparatus

All electrode surface properties were investigated by EIS using a μ-Autolab type III potentiostat (Eco Chemie, Netherlands) with frequency response analyzer (FRA) software. The three-electrode system comprised a platinum wire as the counter electrode (CE), an Ag/AgCl reference electrode (RE) and pencil graphite electrode (PGE) as the working electrode (WE), which served as disposable sensor surfaces.

The electrospinning system consisted of a syringe pump (Pump Systems Inc., USA), and a high-voltage supply was utilized for nanofiber fabrication. The morphological features of the nanofiber-modified PGEs for each parameter were determined using a scanning electron microscope (Carl Zeiss 300VP, Germany).
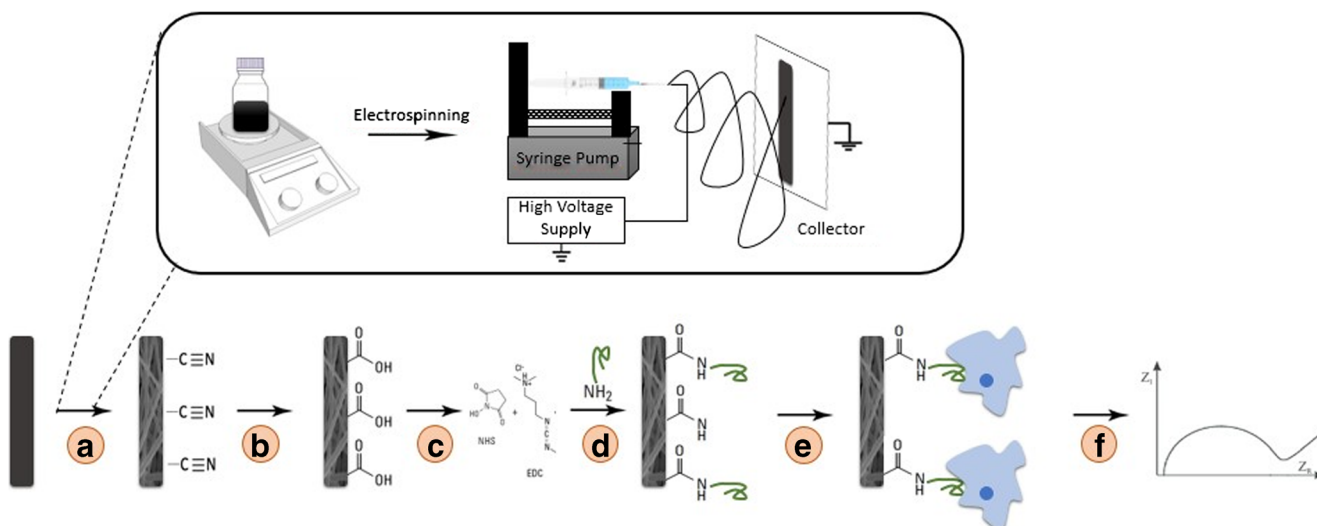
Fig. 1 Schematic illustration of the aptasensor preparation: electrospinning (**a**), chemical activation (**b**), carbodiimide chemistry (**c**), aptamer immobilization (**d**), cell interaction (**e**), EIS transduction (**f**)

All cells used in this study were provided by the American Type Culture Collection (ATCC; Rockville, MD, USA) and cultivated as indicated in the ATCC guideline [see Electronic Supplementary Material (ESM), section S1].

Methods

Stepwise aptasensor preparation

A label-free aptamer-based nanobiosensor has been developed for the direct detection of A549 cells, using a PAN/PPy composite nanofiber-modified PGE as an electrochemical transducer. The aptamer sequence was immobilized on the PAN/PPy nanofiber-modified PGE surface via carbodiimide chemistry. Finally, cancer cell detection was accomplished by EIS transduction of the aptamer–cell interaction.
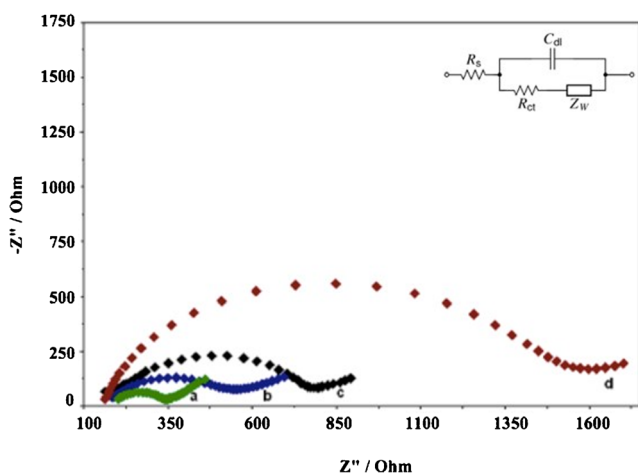

Fig. 2 Nyquist plots obtained from different conditions of the sensor surfaces in the presence of 5 mM $[Fe(CN)_6]^{3-/4-}$ in PBS; before (**a**) and after incubation with aptamer (**b**), interactions with HeLa cell culture (**c**) and target A549 cell culture (**d**) at aptamer-modified f-NFPGE surfaces. Inset: Randles equivalent circuit

Fabrication of nanofibers onto PGEs In order to prepare the polymer solution, 0.369 g (8 wt%) PAN was dissolved in 5 ml DMF until a clear solution was obtained by mechanical stirring. Next, 0.041 g PPy corresponded to ~10 wt% of PAN mass was added to the solution. This PAN/PPy solution was stirred for 7 days at 60 °C to obtain a homogeneous solution [29, 30]. The solution was loaded into a 5-mL syringe connected to a high voltage for the electrospinning process. A fixed voltage of 15 kV and a flow rate of 1.5 mL/h were applied for 1 h at ambient conditions. The distance between the syringe and the collector was kept at 30 cm. As a result, nanofibers were collected directly onto PGEs, and this electrode was denoted as NFPGE.

Functionalization of the NFPGE surfaces To obtain chemically activated carboxyl (–COOH) groups on the surface of the NFPGEs, a literature procedure [31] was applied, with some modifications. For the functionalization process, electrodes were dipped into 2 M NaOH aqueous solution for 1 h at 40 °C to convert nitrile (–CN) groups of PAN to carboxyl (–COOH) and amine (–NH$_2$) groups. Subsequently, carboxyl groups on the NFPGE surface were chemically activated by exposure to PBS solution containing 5 mM EDC and 8 mM NHS used for free amino group coupling. Functionalized NFPGEs were denoted as f-NFPGEs.

Preliminary studies using f-NFPGE surfaces were tested using fish sperm dsDNA to confirm the carboxyl group formation on the nanofibers and to compare DNA binding capacities of each sensor surface. NFPGEs were converted into f-NFPGE surfaces using the aforementioned protocol. Next, 10 μg/mL of dsDNA was covalently immobilized onto bare PGE, NFPGE and f-NFPGE surfaces. Subsequently, differential pulse

Fig. 3 SEM images of PGE (**a**), NFPGE (**b**), aptamer/f-NFPGE (**c**), A549/aptamer/f-NFPGE (**d**) and HeLa/aptamer/f-NFPGE (**e**) at an acceleration voltage of 5.0 kV with a resolution of 2 μm
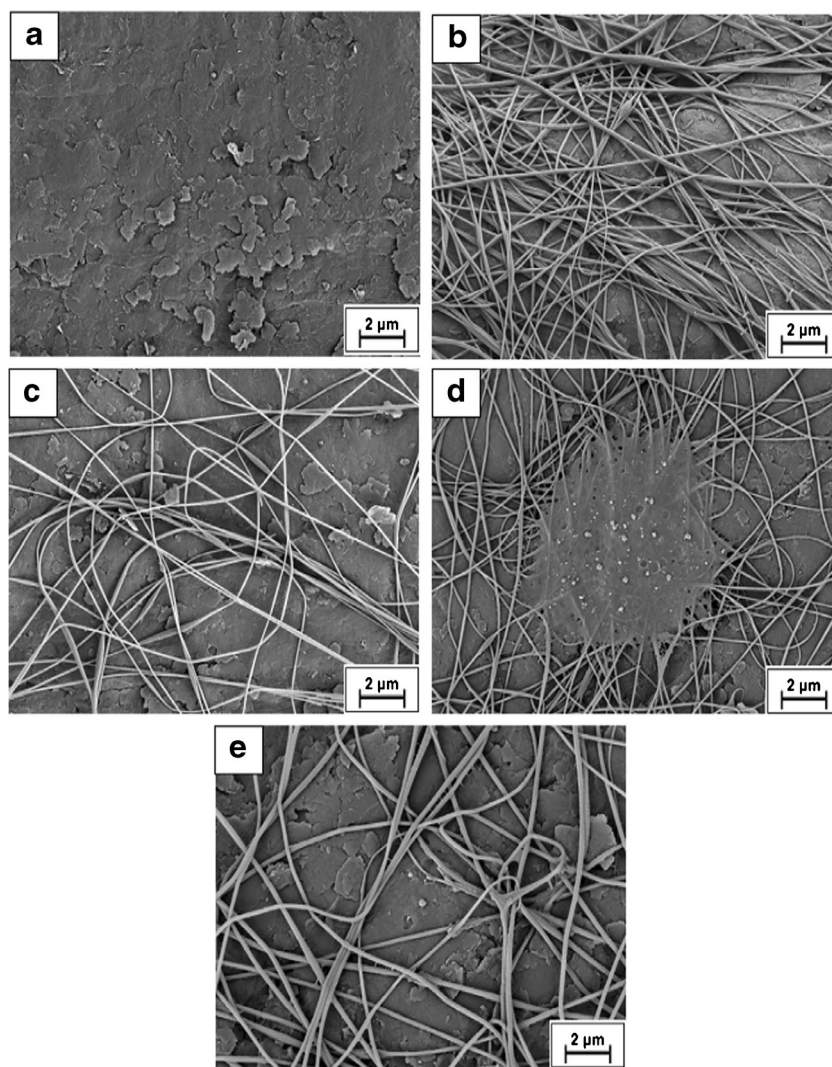
voltammetry (DPV) and electrochemical impedance spectroscopy (EIS) measurements were performed (see ESM section S2). The f-NFPGE surfaces were chosen as optimum sensor surfaces due to carboxyl group formation and resulting high DNA binding capacity (ESM Fig. S1).

Aptamer biomodification Each f-NFPGE was dipped in 100 μL of the desired concentration of the aptamer in 0.50 M ABS for 1 h. Immobilization of the aptamer occurred via formation of covalent bonds between amino groups of the aptamer and carboxyl groups of PAN. Subsequently, each electrode denoted as aptamer/f-NFPGE was dipped in %1 DEA solution in PBS for 1 h to block the nonspecific binding sites of the electrode surfaces.

Target interaction with aptamer Each aptamer/f-NFPGE was dipped into 100 μL of PBS solution including 1×10^5

cells/mL of A549 cell culture at 37.5 °C and 600 rpm for 1 h. To remove unbound cells, each electrode was dipped in 100 μL of PBS for 2 min. To assess the selectivity of the developed aptasensor, human cervical cancer (HeLa) cell culture as a nonspecific target cell was employed by following the same protocol, simultaneously in each trial.

EIS transduction An EIS technique was employed to measure the interactions between the aptamer–A549 target cells and aptamer–HeLa nonspecific target cells. The electrodes were measured by the R_{ct} values in Nyquist plots, in PBS with 0.5 mM $[Fe(CN_6)]^{3-/4-}$ at a potential of 0.24 V. EIS performance parameters included a frequency range of 10 kHz to 50 mHz and an applied AC amplitude of 10 mV. The impedance data were fitted to the Randles equivalent circuit.

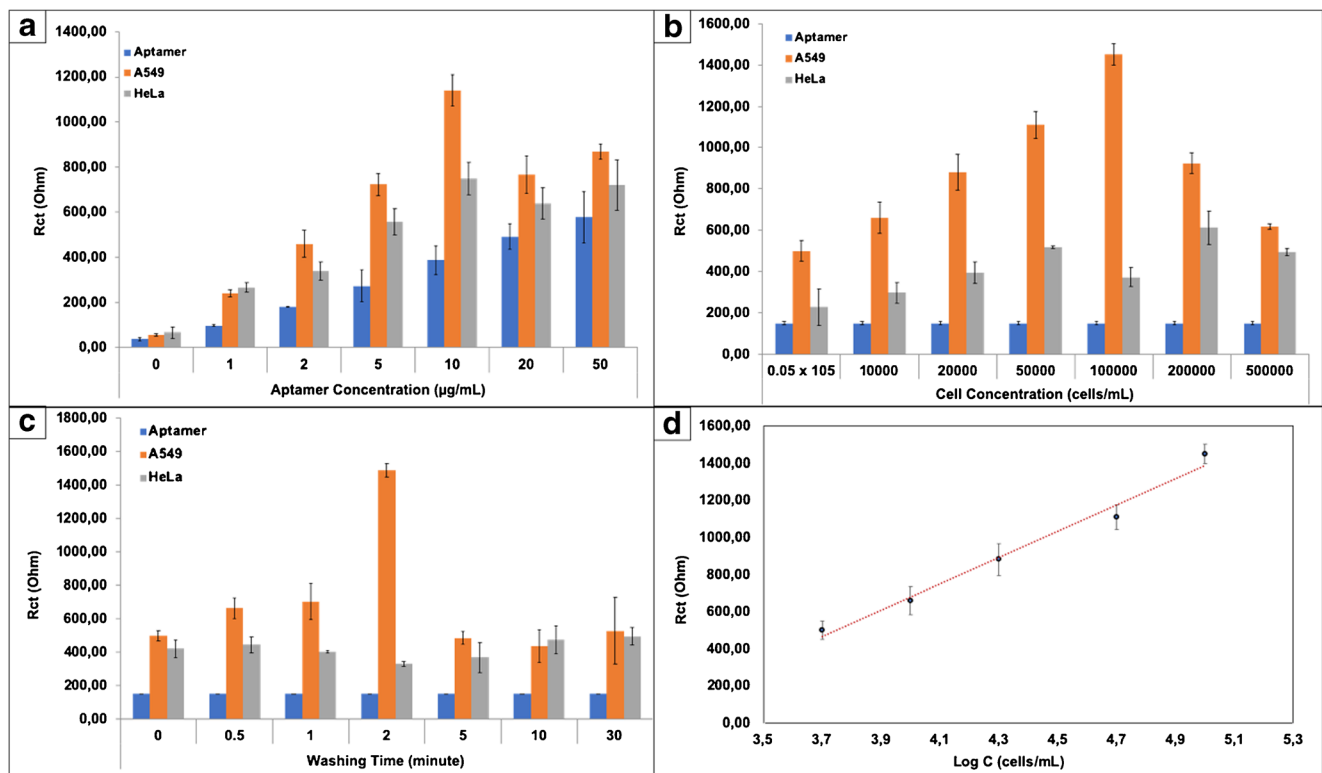A schematic illustration of the study procedure is shown in Fig. 1.

Fig. 4 Histogram charts showing R_{ct} values obtained in the presence of 5 mM $[Fe(CN)_6]^{3-/4-}$ in PBS; aptamer concentration (**a**), cell concentration (**b**), washing time (**c**) and linear calibration plot for R_{ct} vs. log C_{A549} (**d**)

Results and discussion

In this study, a sensitive and selective label-free aptasensor was developed toward non-small cell lung cancer cells. Nanofibers containing 8 wt% PAN and 10 wt% PPy of PAN mass were deposited by electrospinning onto PGEs and used as disposable sensor surfaces. A 5′- aminohexyl-linked aptamer sequence was immobilized onto f-NFPGEs. The interactions between the aptamer and target cells were monitored by EIS transduction.

Characterization of the modified electrodes

The semicircle in high frequency results in a well-defined resistance of charge transfer (R_{ct}) for Faradic reaction, and the diameter of this semicircle is proportional to the R_{ct} value [32, 33]. Characteristic Nyquist plots of each modification of the electrodes are illustrated in Fig. 2. According to the electrochemical characterization results, the corresponding R_{ct} value of bare NFPGEs is estimated to be ~1200 Ω (data not shown). The R_{ct} decreased to 130 Ω (curve a) after

Table 1 Effects of aptamer, cell concentration and washing time on NSCLC detection

		Aptamer concentration (µg/mL)						
		0	1	2	5	10	20	50
$\Delta R_{ct}\%$	A549	34.2	60.3	60.8	62.2	**66.1**	35.7	33.6
	HeLa	43.3	64.1	47.0	51.0	**48.2**	23.1	19.8
		Cell concentration (10^5 cell/mL)						
		0.05	0.1	0.2	0.5	1	2	5
$\Delta R_{ct}\%$	A549	70.4	77.6	83.2	86.7	**89.8**	84.0	76.1
	HeLa	35.0	50.0	62.3	71.4	**60.3**	75.8	70.1
		Washing time (min)						
		0	0.5	1	2	5	10	30
$\Delta R_{ct}\%$	A549	70.1	77.6	78.9	**90.1**	69.5	65.9	71.9
	HeLa	64.7	66.5	63.2	**55.0**	59.5	68.7	70.0

$\Delta R_{ct}\%$ values were calculated for each optimization condition according to the equation $[(Rct_{aptamer + target} - Rct_{aptamer})/Rct_{aptamer + target}] \times 100\%$
Underlined values are the optimized data by specificity and selectivity

functionalization of the NFPGE, due to the formation of carboxyl groups. This decrease is attributed to the high electron density from the double bonds between carbon and oxygen atoms [33]. After covalent immobilization of the aptamer onto the f-NFPGE, the R_{ct} increased to 440 Ω (curve b) as a result of the strong electrostatic repulsion interaction between the aptamer and the redox probe of $[Fe(CN_6)]^{3-/4-}$ [34]. The interaction between the aptamer and A549 cells further increased the R_{ct} value from 440 Ω to 1332 Ω (curve d). This considerable increase occurred due to the insulating properties of biological cells. Therefore, interaction with target cells on the electrode surface inhibited electron transfer, thus resulting in increased R_{ct} values [35]. HeLa cells were used as negative control cells in all experiments to control the selectivity. The incubation of the sensor with HeLa cells resulted in a slight increase in the R_{ct} from 440 Ω to ~525 Ω (curve c), demonstrating the good selectivity of the aptasensor toward A549 cells.

SEM was further used to confirm the selective capture of A549 cells on the nanofiber-modified electrode surface, at an acceleration voltage of 5.0 kV with 2 μm resolution. Typical SEM images of the bare PGE, NFPGE, aptamer/f-NFPGE, A549/aptamer/f-NFPGE and HeLa/aptamer/f-NFPGE are shown in Fig. 3. PPy was used because of its high electrical conductivity surface-to-volume ratio and porosity. PAN was used as a copolymer to enhance the poor solubility and brittleness of PPy [36]. The average diameter of the electrospun

PAN/PPy nanofibers was found to be at about 160 nm. As can be seen in Fig. 3b, nanofiber formation was confirmed in contrast to the bare PGEs (Fig. 3a). As shown in Fig. 3d, A549 cells selectively captured by the aptamer could be observed at the sensor surface. On the other hand, nonspecific HeLa cells were not captured by the aptamer (Fig. 3e), suggesting the excellent selectivity of the sensor toward target A549 cells.

Analytical performance of the aptasensor

To achieve high sensitivity, a series of optimization conditions were tested, including aptamer concentration, cell concentration and washing time (Fig. 4). Different concentrations of the aptamer (1, 2, 5, 10, 20 and 50 μg/mL) were applied on a series of f-NFPGE sensor surfaces at a fixed A549 and HeLa cell concentration of 1×10^5 cells/mL, and the changes in R_{ct} values were evaluated. As the concentration of the aptamer increased, the R_{ct} values increased linearly. At 1 μg/mL aptamer concentration, the sensor's capacity to detect A549 and HeLa cells remained nearly constant, with low selectivity. The sensor was able to detect A549 cells selectively until the aptamer concentration reached 10 μg/mL, at which point the maximum distinction between A549 and HeLa cells was achieved. Thus, an aptamer concentration of 10 μg/mL was chosen as an optimum condition for further examination (Fig. 4a). The effect of cell concentration was determined by
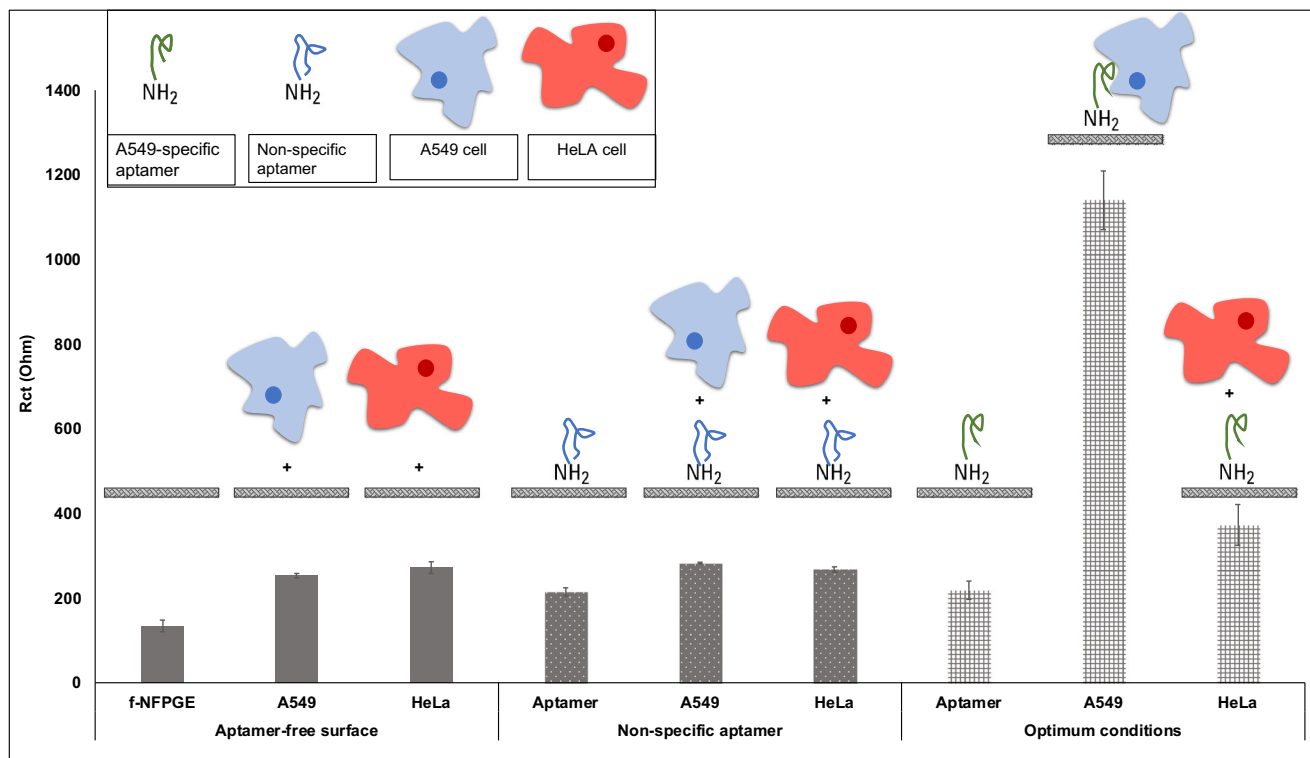

Fig. 5 The comparison of selectivity using aptamer-free and nonspecific aptamer-immobilized sensor surfaces and under optimized conditions of the developed aptasensor and their interactions with target cells

Table 2 Key features of existing electrochemical biosensors for the detection of NSCLC and our aptasensor

Method of detection	Approach	Electrode	Nanomaterial interface	Selective	Ref.
Electrochemical aptasensor	Label-free	Pencil graphite electrode (PGE)	PAN/PPy nanofibers	A549 cells	This work
Electrochemical aptasensor	Label-free	PGE	–	A549 cells	[15]
Electrochemical aptasensor	Label-free	Microfluidic gold chip	–	A549 cells	[38]
Electrochemical aptasensor	Sandwich assay	Glassy carbon electrode (GCE)	Gold nanoparticles (AuNPs)	MUC-1-positive A549 cells	[39]
Electrochemical aptasensor	Label-free	Carbon-based screen-printed electrode (SPE)	Carbon-gold nanocomposite	VEGF$_{165}$ biomarker	[34]
Electrochemical DNA-sensor	Signal-on	Gold disk electrode	AuNPs	microRNA	[40]
Electrochemical DNA-sensor	Signal-on	GCE	Graphene oxide (GO)/CuO nanocomposite	CYFRA21-1 biomarker	[41]
Electrochemical immunosensor	Sandwich assay	GCE	Graphene/chitosan/glutaraldehyde composite	CYFRA21-1 biomarker	[42]
Electrochemical immunosensor	Label-free	GCE	AuNP/reduced graphene oxide (rGO)/chitosan composite	Neuron-specific enolase (NSE)	[43]

increasing each concentration (0.1, 0.2, 0.5, 1, 2 and 5×10^5 cells/mL) of the A549 and HeLa cells at the fixed 10 μg/mL aptamer concentration applied to the surfaces. The highest analytical response for the A549–aptamer interaction was observed when the A549 cell culture was diluted to 1×10^5 cells/mL. In addition, at this concentration, the HeLa–aptamer non-specific interaction was mostly hindered, and thus the highest selectivity toward A549 cells was obtained (Fig. 4b). Because washing of the modified sensor after cell interaction could directly affect the electrochemical signal, the effect of increasing washing time (0, 0.5, 1, 2, 5, 10 and 30 min) of cells was evaluated. At washing time of 2 min, most of the nonspecific HeLa cells were eliminated, and high selectivity toward A549 cells was observed. Thus, 2 min was selected as the optimum washing time.

As shown in Table 1, $\Delta R_{ct}\%$ values were calculated for each optimization condition according to the given equation:

$$\left[\left(Rct_{aptamer+target} - Rct_{aptamer}\right)/Rct_{aptamer+target}\right] \times 100\%.$$

$Rct_{aptamer + target}$ (Rct_{A549} and Rct_{HeLa}) values were attributed to the charge transfer resistance obtained after the interaction between the aptamer and the target cells. $Rct_{aptamer}$ is the resistance obtained after immobilization of the aptamer on the f-NFPGE surfaces. The difference between these values indicated the specificity and selectivity of the aptasensor. The R_{ct} value was proportional to the logarithmic value of A549 cell concentration over the range of 5×10^3 cells/mL to 1×10^5 cells/mL. The linear regression equation was R_{ct} $(Ohm) = -2170.6 + 712.15$ Log[C], with a correlation coefficient (R^2) of 0.98. The limit of detection was calculated to be 1.2×10^3 cells/mL ($S/N = 3$).

Next, the selectivity and specificity of the aptamer toward A549 cells was confirmed by altering the biorecognition part of the developed aptasensor using aptamer-free and nonspecific aptamer-immobilized sensor surfaces. Control cell HeLa and target cell A549 were respectively left for incubation onto each sensor surfaces under optimum conditions by employing the aforementioned method. The results indicate that the R_{ct} value only increased after the interaction between the A549-specific aptamer and A549 cells (Fig. 5). R_{ct} responses obtained over aptamer-free and nonspecific aptamer-immobilized surfaces led to no obvious changes. Thus, it has been proven that the developed aptasensor can be utilized to distinguish between A549 cells and a negative control cell.

The stability of the NFPGE surfaces was tested by evaluating the ΔR_{ct} values obtained under optimized conditions after interaction with A549 and HeLa cells at the aptamer-coated f-NFPGE surfaces on days 1, 7, 15 and 30 (ESM, section S3). When not in use, NFPGE surfaces were stored at room temperature. The ΔR_{ct} values were calculated according to A549 cell binding retained (96% at 7th day, 78% at 15th

day and 25% at 30th day,) in comparison with values on the first day. The aptasensor also retained the selectivity, with HeLA cell binding of 74%, 64% and 6% for days 7, 15 and 30, respectively (ESM Fig. S2).

Various electrochemical methods for the detection of NSCLC disease in terms of cell-based or related biomarkers are shown in Table 2. As can be seen, biomarker-related electrochemical biosensors are more common, although cancer cell detection has numerous advantages over them. The main drawback of biomarker-related biosensors is that these molecules are not recommended individually for clinical diagnosis [6]. With the integration of aptamer molecules into cell-based electrochemical detection methods, convenient methods for cell counting, cell classification and detection of cancer cells, even at an early stage, can be achieved [37].

Aptasensor response to dead cells

Cultured cell lines were used as target molecules in this study. A series of trials were conducted in order to eliminate the cell culture process and thus increase the applicability of the sensor to real human samples. Three types of death protocols were used, as follows: UV-controlled death, spontaneous death and death with lysis solution (lysates). Sensor capacity was evaluated by investigating the interactions between aptamer and dead cancer cells. Figure 6A shows the R_{ct} values after interaction with living A549 and HeLA cells and dead cells at aptamer-modified surfaces. As can be seen from the histogram chart, the developed aptasensor was able to properly detect cultured cell lines.

Figure 6B shows the morphology of the cells as follows: (a) living A549, (b) living HeLa, (c) UV-controlled dead A549,

(d) UV-controlled dead HeLa, (e) spontaneously dead A549, (f) spontaneously dead HeLa, (g) lysed A549 and (h) lysed HeLa cell lines. The cell membrane integrity was ruptured due to the lysis process, and thus the aptamer was not able to capture the cells. Also, A549 cells could not be captured when spontaneous cell death occurred through the presence of bacterial growth. Finally, the cells tended to form clustered structures when exposed to UV light, which enhanced the capacity of the sensor to detect A549 cells, but nonspecific recognition of HeLa cells was also observed, which led to loss of selectivity.

Conclusion

In summary, a sensitive and selective label-free electrochemical aptasensor was developed for the detection of human non-small cell lung cancer cells (A549) using PAN/PPy nanofiber-modified PGE sensor surfaces. Both A549 target cells and nonspecific HeLa were introduced to the aptamer-immobilized f-NFPGE surfaces, and the differences in R_{ct} values were evaluated. Selectivity was also controlled by altering the bioreceptor part. Aptamer-free and nonspecific aptamers were used for this purpose, and their interactions with target cells were monitored using an EIS technique. The aptasensor showed a very low detection limit of 1.2×10^3 cells/mL specifically toward A549 cells, due to the modification of the PGE with PAN/PPy nanofibers. This study shows that the integration of aptamers into electrochemical biosensors holds great promise as a cost-effective and robust technique, with high sensitivity and specificity, for the early diagnosis of cancer.
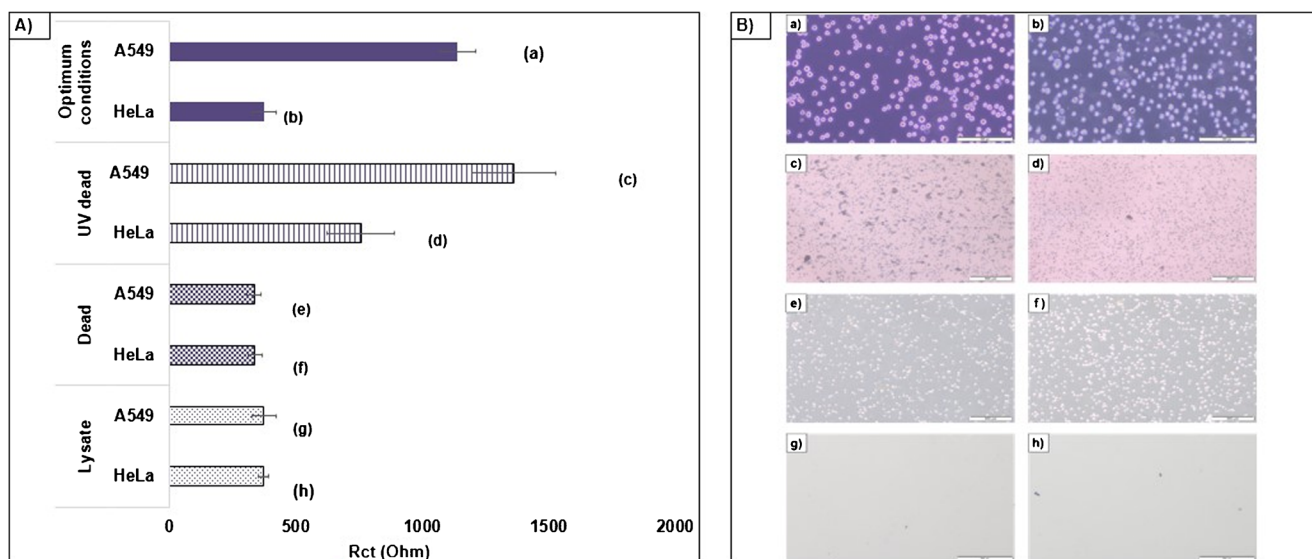

Fig. 6 a R_{ct} values obtained in the presence of 5 mM $[Fe(CN)_6]^{3-/4-}$ interactions with living, UV-controlled dead, spontaneously dead and lysate A549 and HeLa cells at aptamer-modified surfaces. **b** Morphology images of living (**a**) A549, (**b**) HeLa; UV-controlled dead (**c**) A549, (**d**) HeLa; spontaneously dead (**e**) A549, (**f**) HeLa; lysates of (**g**) A549, (**h**) HeLa cell lines

Compliance with ethical standards

Ethical approval This article does not contain any studies with human participants or animals.

Conflict of interest The authors declare that they have no conflict of interest.

References

1. Jemal A, Bray F, Center MM, Ferlay J, Ward E, Forman D. Global cancer statistics. CA Cancer J Clin. 2011;61(2):69–90. https://doi.org/10.3322/caac.20107.

2. WHO. Cancer. 2018. https://www.who.int/news-room/fact-sheets/detail/cancer. Accessed 12 Nov 2019.

3. Zappa C, Mousa SA. Non-small cell lung cancer: current treatment and future advances. Transl Lung Cancer Res. 2016;5(3):288–300. https://doi.org/10.21037/tlcr.2016.06.07.

4. Lemjabbar-Alaoui H, Hassan O, Yang YW, Buchanan P. Lung cancer: biology and treatment options. Biochim Biophys Acta (BBA) - Rev Cancer. 2015;1856(2):189–210. https://doi.org/10.1016/j.bbcan.2015.08.002.

5. Chen HW, Medley CD, Sefah K, Shangguan D, Tang Z, Meng L, et al. Molecular recognition of small-cell lung cancer cells using aptamers. ChemMedChem. 2008;3(6):991–1001. https://doi.org/10.1002/cmdc.200800030.

6. Wang L. Screening and biosensor-based approaches for lung cancer detection. Sensors. 2017;17(10):2420. https://doi.org/10.3390/s17102420.

7. Ellington AD, Szostak JW. Selection in vitro of single-stranded DNA molecules that fold into specific ligand-binding structures. Nature. 1992;355(6363):850–2. https://doi.org/10.1038/355850a0.

8. Baird GS. Where are all the aptamers? Am J Clin Pathol. 2010;13(4):529–31. https://doi.org/10.1309/AJCPFU4CG2WGJJKS.

9. Zhang Y, Lai B, Juhas M. Recent advances in aptamer discovery and applications. Molecules. 2019;24(5):941. https://doi.org/10.3390/molecules24050941.

10. Kaur H, Bruno JG, Kumar A, Sharma TK. Aptamers in the therapeutics and diagnostics pipelines. Theranostics. 2018;8(15):4016–32. https://doi.org/10.7150/thno.25958.

11. Kara P, De la Escosura-Muñiz A, Maltez-da Costa M, Guix M, Ozsoz M, Merkoçi A. Aptamers based electrochemical biosensor for protein detection using carbon nanotubes platforms. Biosens Bioelectron 2010;26(4):1715–1718. https://doi.org/10.1016/j.bios.2010.07.090.

12. Figueroa-Miranda G, Feng L, Chi-Chin Shiu S, Dirkzwager RM, Cheung YW, Tanner JA, et al. Aptamer-based electrochemical biosensor for highly sensitive malaria detection with adjustable dynamic response range and reusability. Sensors Actuators B Chem. 2018;255(1):235–43. https://doi.org/10.1016/j.snb.2017.07.117.

13. Rivas L, Mayorga-Martinez CC, Quesada-Gonzáles D, Zamora-Gálvez A, De la Escosura-Muñiz A, Merkoçi A. Label-free Impedimetric Aptasensor for Ochratoxin-a detection using iridium oxide nanoparticles. Anal Chem 2015;87(10):5167–5172. https://doi.org/10.1021/acs.analchem.5b00890.

14. Li X, Cheng R, Shi H, Tang B, Xiao H, Zhao G. A simple highly sensitive and selective aptamer-based colorimetric sensor for environmental toxins microcystin-LR in water samples. J Hazardous Materails. 2016;304(5):474–80. https://doi.org/10.1016/j.jhazmat.2015.11.016.

15. Kara P, Erzurumlu Y, Ballar Kirmizibayrak P, Ozsoz M. Electrochemical aptasensor design for label free cytosensing of human non-small cell lung cancer. J Electroanal Chem. 2016;775:337–41. https://doi.org/10.1016/j.jelechem.2016.06.008.

16. Sun D, Lu J, Chen D, Jiang Y, Wang Z, Qin W, et al. Label-free electrochemical detection of HepG2 tumor cells with a self-assembled DNA nanostructure-based aptasensor. Sensors Actuators B Chem. 2018;268(1):359–67. https://doi.org/10.1016/j.snb.2018.04.142.

17. Shen H, Yang J, Chen Z, Chen X, Wang L, Hu J, et al. A novel label-free and reusable electrochemical cytosensor for highly sensitive detection and specific collection of CTCs. Biosens Bioelectron. 2016;81(15):495–502. https://doi.org/10.1016/j.bios.2016.03.048.

18. Sun H, Zu Y. A highlight of recent advances in aptamer technology and its application. Molecules. 2015;20(7):11959–80. https://doi.org/10.3390/molecules200711959.

19. Hong P, Li W, Li J. Applications of aptasensors in clinical diagnostics. Sensors. 2012;12(2):1181–93. https://doi.org/10.3390/s120201181.

20. Thévenot DR, Toth K, Durst RA, Wilson GS. Electrochemical biosensors: recommended definitions and classification. Biosens Bioelectron. 2001;16(1–2):121–31. https://doi.org/10.1016/S0956-5663(01)00115-4.

21. Dolatabadi JEN, Mashinchian O, Ayoubi B, Jamali AA, Mobed A, Losic D, et al. Optical and electrochemical DNA nanobiosensors. TrAC Trends Anal Chem. 2011;30(3):459–72. https://doi.org/10.1016/j.trac.2010.11.010.

22. Cho EJ, Lee JW, Ellington AD. Applications of aptamers as sensors. Annu Rev Anal Chem. 2009;2(1):241–64. https://doi.org/10.1146/annurev.anchem.1.031207.112851.

23. Song KM, Lee S, Ban C. Aptamers and their biological applications. Sensors. 2012;12(1):612–31. https://doi.org/10.3390/s120100612.

24. Wang R, Di J, Ma J, Ma Z. Highly sensitive detection of cancer cells by electrochemical impedance spectroscopy. Electrochim Acta. 2012;61:179–84. https://doi.org/10.1016/j.electacta.2011.11.112.

25. Lisdat F, Schäfer D. The use of electrochemical impedance spectroscopy for biosensing. Anal Bioanal Chem. 2008;391:1555–67. https://doi.org/10.1007/s00216-008-1970-7.

26. Jun J, Lee JS, Shin DH, Jang J. Aptamer-functionalized hybrid carbon nanofiber FET-type electrode for a highly sensitive and selective platelet-derived growth factor biosensor. ACS Appl Mater Interfaces. 2014;6(16):13859–65. https://doi.org/10.1021/am5032693.

27. Yang Y, Yang X, Yang X, Yang Y, Yuan Q. Aptamer-functionalized carbon nanomaterials electrochemical sensors for detecting cancer relevant biomolecules. Carbon. 2018;129. https://doi.org/10.1016/j.carbon.2017.12.013.

28. Zhao Z, Xu L, Shi X, Tan W, Fang X, Shangguan D. Recognition of subtype non-small cell lung cancer by DNA aptamers selected from living cells. Analyst. 2009;134(9):1808–14. https://doi.org/10.1039/b904476k.

29. Ince Yardimci A, Baskan O, Yilmaz S, Mese G, Ozcivici E, Selamet Y. Osteogenic differentiation of mesenchymal stem cells on random and aligned PAN/PPy nanofibrous scaffolds. J Biomed Appl. 2019;34(5):640–50. https://doi.org/10.1177/0885328219865068.

30. Ji L, Yao Y, Toprakci O, Lin Z, Liang Y, Shi Q, et al. Fabrication of carbon nanofiber-driven electrodes from electrospun

polyacrylonitrile/polypyrrole bicomponents for high-performance rechargeable lithium-ion batteries. J Power Sources. 2010;195(7):2050–6. https://doi.org/10.1016/j.jpowsour.2009.10.021.

31. Gupta PK, Gupta A, Dhakate S, Khan ZH, Solanki PR. Functionalized polyacrylonitrile-nanofiber based immunosensor for Vibrio cholerae detection. J Appl Polym Sci. 2016;133(44). https://doi.org/10.1002/app.44170.

32. Muñoz J, Montes R, Baeza M. Trends in electrochemical impedance spectroscopy involving nanocomposite transducers: characterization, architecture surface and bio-sensing. TrAC. 2017;97:201–15. https://doi.org/10.1016/j.trac.2017.08.012.

33. Li LX, Li F. The effect of carbonyl, carboxyl and hydroxyl groups on the capacitance of carbon nanotubes. New Carbon Mat. 2011;26(3):224–8. https://doi.org/10.1016/S1872-5805(11)60078-4.

34. Tabrizi MA, Shamsipur M, Farzin L. A high sensitive electrochemical aptasensor for the determination of VEGF165 in serum of lung cancer patient. Biosens Bioelectron. 2015;74:764–269. https://doi.org/10.1016/j.bios.2015.07.032.

35. Pan C, Guo M, Nie Z, Xiao X, Yao S. Aptamer-based electrochemical sensor for label-free recognition and detection of cancer cells. Electroanalysis. 2009;22(11):1321–6. https://doi.org/10.1002/elan.200804563.

36. Jun TS, Ho TA, Rashid M, Kim YS. A novel methanol sensor based on gas-penetration through a porous Polypyrrole-coated Polyacrylonitrile nanofiber mat. J Nanosci Nanotechnol. 2013;13(9):6249–53. https://doi.org/10.1166/jnn.2013.7693.

37. Zhang Z, Li Q, Liu M. Application of electrochemical biosensors in tumor cell detection. Thorac Cancer. 2020;11(4):840–50. https://doi.org/10.1111/1759-7714.13353.

38. Mir TA, Yoon JH, Gurudatt NG, Won MS, Shim YB. Ultrasensitive cytosensing based on an aptamer modified nanobiosensor with a bioconjugate: detection of human non-small-cell lung cancer cells. Biosens Bioelectron. 2015;74(15):594–600. https://doi.org/10.1016/j.bios.2015.07.012.

39. Nguyen NV, Yang CH, Liu CJ, Kuo CH, Wu DC, Jen CP. An aptamer-based capacitive sensing platform for specific detection of lung carcinoma cells in the microfluidic chip. Biosensors (Basel). 2018;8(4):98. https://doi.org/10.3390/bios8040098.

40. Liu S, Su W, Li Z, Ding X. Electrochemical detection of lung cancer specific microRNAs using 3D DNA origami nanostructures. Biosens Bioelectron. 2015;71:57–61. https://doi.org/10.1016/j.bios.2015.04.006.

41. Chen M, Hou C, Huo D, Yang M, Fa H. A highly sensitive electrochemical DNA biosensor for rapid detection of CYFRA21-1, a marker of non-small cell lung cancer. Anal Methods. 2015;7(22):9466–73. https://doi.org/10.1039/C5AY02505B.

42. Zeng Y, Bao J, Zhao Y, Huo D, Chen M, Qi Y, et al. A sandwich-type electrochemical immunoassay for ultrasensitive detection of non-small cell lung cancer biomarker CYFRA21-1. Bioelectrohemistry. 2018;120:183–9. https://doi.org/10.1016/j.bioelechem.2017.11.003.

43. Wei Z, Zhang J, Zhang A, Wang Y, Cai X. Electrochemical detecting lung cancer-associated antigen based on graphene-gold nanocomposite. Molecules. 2017;22(3):392. https://doi.org/10.3390/molecules22030392.